Macrophage Scavenger Receptor 1 mediates lipid-induced inflammation in non-alcoholic fatty liver disease

Olivier Govaere[1], Nuria Martinez-Lopez[2,3†], Sine Kragh Petersen[4†], Rosellina M. Mancina[5], Oveis Jamialahmadi[5], Pierre Bel Lassen[6], Rebecca Darlay[7], Julien Peltier[2], Ramy Younes[1,8], Dina Tiniakos[1,9], Guruprasad P. Aithal[10], Michael Allison[11], Michele Vacca[12], Hannele Yki-Järvinen[13], Jean-Francois Dufour[14], Mattias Ekstedt[15], Sven Francque[16], Salvatore Petta[17], Elisabetta Bugianesi[8], Jörn M Schattenberg[18], Christopher P. Day[1], Heather J. Cordell[7], Karine Clément[6], Stefano Romeo[5], Vlad Ratziu[19], Ann K. Daly[1], Quentin M. Anstee[1,20]*, Matthias Trost[2]*, Anetta Härtlova[2,4]*

[1]Translational and Clinical Research Institute, Faculty of Medical Sciences, Newcastle University, Newcastle upon Tyne, United Kingdom.

[2]Biosciences Institute, Faculty of Medical Sciences, Newcastle University, Newcastle upon Tyne, United Kingdom.

[3]Department of Medicine, Albert Einstein College of Medicine, New York, USA,

[4]Wallenberg Centre for Molecular and Translational Medicine, Department of Microbiology and Immunology at Institute of Biomedicine, University of Gothenburg, Gothenburg, Sweden.

[5]The Wallenberg Laboratory for Cardiovascular and Metabolic Research, Department of Molecular and Clinical Medicine, University of Gothenburg, Gothenburg, Sweden.

[6] Nutrition and obesity: systemic approaches, Inserm, Sorbonne University, Paris, France.

[7]Population Health Sciences Institute, Faculty of Medical Sciences, Newcastle University, Newcastle upon Tyne, United Kingdom.

[8]Department of Medical Sciences, Division of Gastro-Hepatology, A.O. Città della Salute e della Scienza di Torino, University of Turin, Turin, Italy.

[9] Department of Pathology, Aretaieio Hospital, National & Kapodistrian University of Athens, Athens, Greece.

[10]NIHR Nottingham Biomedical Research Centre, Nottingham University Hospitals NHS Trust and University of Nottingham, Nottingham, United Kingdom.

[11]Liver Unit, Department of Medicine, Cambridge Biomedical Research Centre, Cambridge University NHS Foundation Trust, United Kingdom.

[12]University of Cambridge Metabolic Research Laboratories, Wellcome-MRC Institute of Metabolic Science, Addenbrooke's Hospital, Cambridge, United Kingdom.

[13]Department of Medicine, University of Helsinki, Helsinki, Finland.

[14]University Clinic for Visceral Surgery and Medicine, University of Berne, Freiburgstrasse, Berne, Switzerland.

[15]Division of Gastroenterology and Hepatology, Department of Medicine and Health Sciences, Linköping University, Linkoping, Sweden.

[16]Department of Gastroenterology and Hepatology, Antwerp University Hospital & University of Antwerp, Antwerp, Belgium.

[17]Sezione di Gastroenterologia, Dipartimento Biomedico di Medicina Interna e Specialistica, Università di Palermo, Palermo, Italy.
[18]I. Department of Medicine, University Hospital Mainz, Mainz, Germany.
[19]Assistance Publique-Hôpitaux de Paris, hôpital Beaujon, University Paris-Diderot, Paris, France.
[20] Newcastle NIHR Biomedical Research Centre, Newcastle upon Tyne Hospitals NHS Trust, Newcastle upon Tyne, United Kingdom.

† Contributed equally

*Correspondence:
Dr Anetta S. Härtlova, PhD
Assistant Professor
Wallenberg Centre for Molecular and Translational Medicine
University of Gothenburg, Institute of Biomedicine
Department of Microbiology and Immunology
Medicinaregatan 7 A
40530 Göteborg
Sweden
Email: anetta.hartlova@gu.se

Prof Matthias Trost, PhD
Biosciences Institute,
The Medical School, Newcastle University,
4th Floor, William Leech Building,
Framlington Place,
Newcastle-upon-Tyne, NE2 4HH,
United Kingdom
Email:matthias.trost@newcastle.ac.uk

Prof Quentin M. Anstee, PhD, FRCP
Translational and Clinical Research Institute,
The Medical School, Newcastle University,
4th Floor, William Leech Building,
Framlington Place,
Newcastle-upon-Tyne, NE2 4HH,
United Kingdom
Email: quentin.anstee@ncl.ac.uk

Abstract:

Obesity-associated inflammation is a key player in the pathogenesis of non-alcoholic fatty liver disease (NAFLD), however the exact mechanisms remain incompletely understood. Here we demonstrate that macrophage scavenger receptor 1 (MSR1) is associated with the occurrence of hepatic lipid-laden foamy macrophages and correlates with the degree of steatosis and steatohepatitis in a large cohort of NAFLD patients. Mice lacking Msr1 are protected against high fat diet-induced metabolic disorder, showing less hepatic inflammation and fibrosis, reduced circulating fatty acids, increased lipid storage in the adipocytes and improved glucose tolerance. Moreover, MSR1 triggers diet-induced JNK-mediated inflammatory activation of macrophages independent of lipopolysaccharide. Taken together, our data suggest a critical role for MSR1 in lipid homeostasis and a potential therapeutic target for the treatment of NAFLD.

One Sentence Summary:

The immunometabolic role of MSR1 in human NAFLD.

Main Text:

With the increasing prevalence of obesity, non-alcoholic fatty liver disease (NAFLD) has become the most common chronic liver disease globally (*1*). NAFLD is characterised by excessive hepatic triglyceride accumulation and represents a series of diseased states ranging from isolated steatosis (non-alcoholic fatty liver, NAFL) to non-alcoholic steatohepatitis (NASH), identified by the presence of necro-inflammation and hepatocyte ballooning, with varying degrees of fibrosis. NAFLD is strongly linked with metabolic syndrome, i.e. dyslipidemia, hypertension, obesity and type 2 diabetes mellitus (T2DM), and currently affects 20 to 30% of the global population (*2*). Importantly, not all patients progress from NAFL to NASH and although gene signatures of more advanced fibrosing-steatohepatitis have been identified, the exact pathogenic pathways involved in the initiating phases of the disease, especially the transition from NAFL to NASH, are not fully understood (*3*).

Growing evidence supports the view that Kupffer cells, the endogenous hepatic macrophages, are initiators of inflammation and hence contribute to NAFLD development, while recruited monocyte-derived macrophages play a crucial role in the disease progression (*4-6*). Hepatic macrophages are responsive to a variety of stimuli including bacterial endotoxins (lipopolysaccharide, LPS) but also free fatty acids (FFAs) or cholesterol (*4-6*). However, molecular mechanisms underlying hepatic macrophage activation remain poorly understood. Recent data show that pro-inflammatory activation of macrophages by saturated fatty acids (SFA) is independent of Toll-like receptor 4, yet the receptor that is responsible is still not known (*7*). Recently, we have shown that *in vitro* activation of the phagocytic receptor, macrophage scavenger receptor 1 (MSR1, also known as SR-A or CD204), results in pro-inflammatory macrophage polarisation through JNK activation *(8)*. MSR1 is a key macrophage receptor for the clearance of circulating lipoproteins and has been implicated in atherogenesis (*9, 10*). We therefore hypothesised that MSR1 might be involved in inflammatory responses in the context of lipid overload during obesity-induced NAFLD.

To investigate the impact of MSR1 on NAFLD, we first analysed *MSR1* gene expression in a cohort of 170 histologically characterised human liver biopsies using nanoString®. The cohort was stratified according to histopathological disease grade and stage, i.e. NAFL and NASH with fibrosis ranging from F0 to F4 (**Table S1**). The analysis revealed a significant increase of *MSR1* gene expression in NASH compared to NAFL, indicating a positive correlation with the active

inflammatory form of the disease (**Fig. 1a**). This observation was supported by a significant correlation between *MSR1* mRNA levels and steatosis grade (r=0.29, p=0.0001), hepatocyte ballooning (r=0.22, p<0.01) and lobular inflammation (r=0.24, p<0.01), while there was no correlation with stages of hepatic fibrosis indicating that *MSR1* mRNA levels are strongly linked to steatohepatitis activity rather than wound healing *per se* (**Fig. 1b and Fig. S1a**) (*11*). Furthermore, *MSR1* levels positively correlated with serum levels of alanine transaminase, ALT (r=0.31, p=0.0001), and aspartate transaminase, AST (r=0.32, p<0.0001) (**Fig. S1b**).

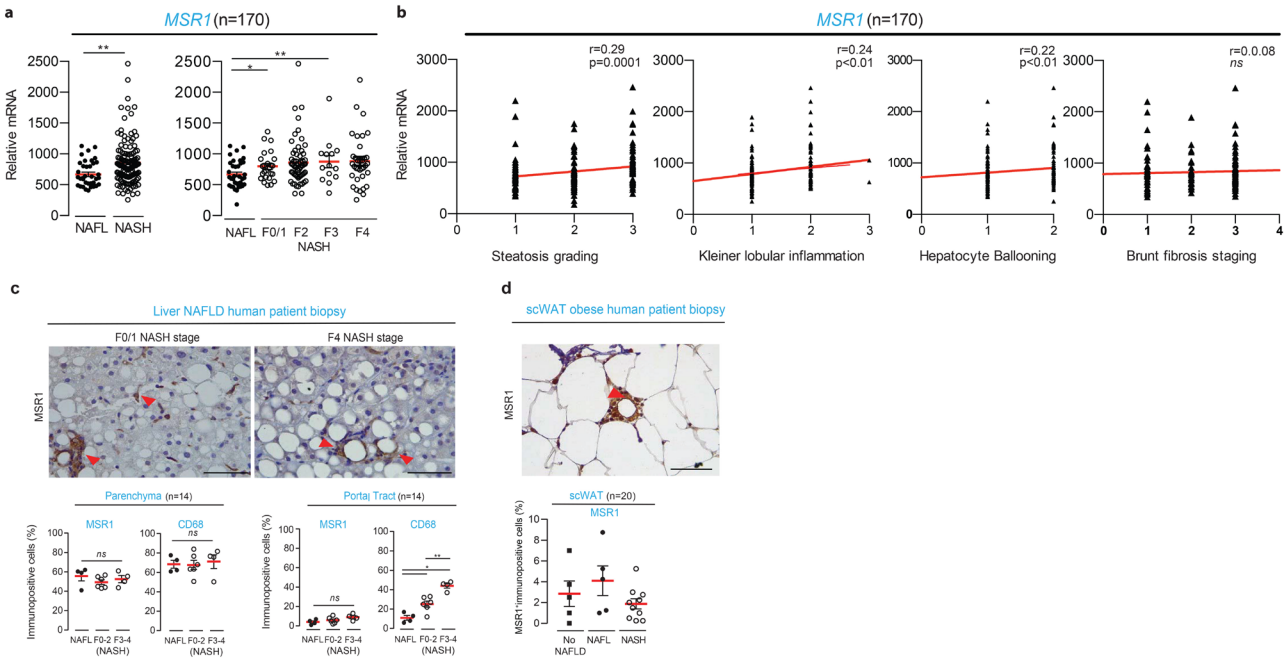

Fig. 1. Macrophage Scavenger Receptor 1 (MSR1) expression in human non-alcoholic fatty liver disease (NAFLD) correlates with steatosis and steatohepatitis. (**a**) mRNA levels of MSR1 in a cohort of 170 histological proven NAFLD samples covering the different stages of the disease (NAFL non-alcoholic fatty liver; NASH non-alcoholic steatohepatitis F0-4 fibrosis stage) using nanoString®. Filled symbols, NAFL stage; open symbols, NASH stage. (**b**) Correlation of *MSR1* gene expression with the steatosis, hepatocyte ballooning, lobular inflammation and fibrosis stage (Spearman correlation) (**c**) The immunohistochemical analysis of MSR1 in liver tissue of human NAFLD patient biopsies (n=14), red arrows indicate foamy macrophages and lipogranuloma. Histopathological quantification of MSR1 and CD68 immunopositive cells in the parenchyma and portal tract of human NAFLD samples with mild and advanced fibrosis (NAFL n=4; NASH F0-2 n=6; NASH F3-4 n=4). (**d**) The immunohistochemical analysis for MSR1 in subcutaneous white adipose tissue (scWAT) from obese patients (n=20). Histopathological

quantification of immunopositive cells in the scWAT was stratified based on the presence of NAFLD (n=20). Data are presented as mean ± SEM (Mann-Whitney-U test, * $p<0.05$, ** $p<0.01$, *** $p<0.001$, **** $p<0.0001$, *ns:* non-significant). Scale bars 200µm.

Histopathological analysis of human NAFLD liver biopsies showed that MSR1 was predominantly expressed in resident liver macrophages rather than infiltrating monocyte-derived macrophages located in the portal tract, as visualised by the CD68 immunostaining (**Fig. 1c and Fig. S2**) (*12, 13*). Notably, MSR1 immunopositivity was seen in lipid-laden foamy macrophages and lipogranulomas throughout the spectrum of NAFLD, indicating a role for MSR1 in lipid accumulation in macrophages and concordantly inflammation (**Fig. 1c and Fig. S2**). As macrophages have been reported to regulate metabolic homeostasis in adipose tissue (*14*), we evaluated MSR1 expression in subcutaneous and matched omental adipose tissue from obese patients (BMI >30 kg/m^2). MSR1-immunopositive macrophages were observed in crown-like structures in both types of adipose tissue, with increased levels of MSR1 in obese patients diagnosed with NAFL (**Fig. 1d and Fig. S2c**). Taken together, these human data demonstrate a positive correlation of MSR1 transcript and protein levels with obesity-associated NAFLD and occurrence of hepatic- and adipose tissue-resident lipid-laden macrophages in the presence of excess lipid accumulation.

To further investigate how MSR1 functionally contributes to the development of obesity-related NAFLD, we subjected *Msr1*$^{-/-}$ mice and their corresponding *Msr1*$^{+/+}$ (wild-type, WT) male and age-matched counterparts to a high-fat and high-cholesterol diet (HFD) for 16 weeks. Upon HFD feeding, *Msr1*-deficient mice displayed an increased total body weight and an increase in liver and epididymal white adipose tissue (eWAT) weight compared to WT (**Fig. 2a-b**). Consistently with enhanced adipose mass, HFD-fed *Msr1*$^{-/-}$ mice displayed larger adipocytes along with enhanced fatty acid accumulation within the cells and increased leptin serum levels compared to WT mice, indicating an increased adiposity and fat storage in the absence of *Msr1* (**Fig. 2c-d, Fig. S3a-b**). To further test the effect of *Msr1*-deficiency on the metabolic syndrome, we measured several parameters within the serum as well as in the eWAT and liver tissue. HFD-fed *Msr1*$^{-/-}$ mice exhibited lower concentrations of circulating FFAs which corresponded to reduced hepatic triglycerides (TGs) and enhanced lipid utilization measured by approximately 50% higher mitochondrial oxygen consumption rate in the liver compared to HFD-fed WT mice (*15*), while

circulating TG levels remained unchanged (**Fig. 2e-f, Fig. S3a-b**). Moreover, the absence of *Msr1* improved glucose uptake from blood in obese mice (**Fig. S3c-e**). Although no murine models accurately recapitulate all histological features of human steatohepatitis (*16*), histological and transcriptomic features of liver fibrosis were clearly attenuated by *Msr1* deficiency (**Fig. 2g-h**). Specifically, less fibrosis, a hallmark of NASH development, and reduced transforming growth factor beta 1 (*Tgfb1*) and alpha-smooth muscle actin (*Acta1*) expression was observed under HFD conditions compared to WT (**Fig. 2i**). Taken together, these results demonstrate that *Msr1* deficiency increases the body weight but protects against HFD-associated metabolic dysregulation and liver damage.

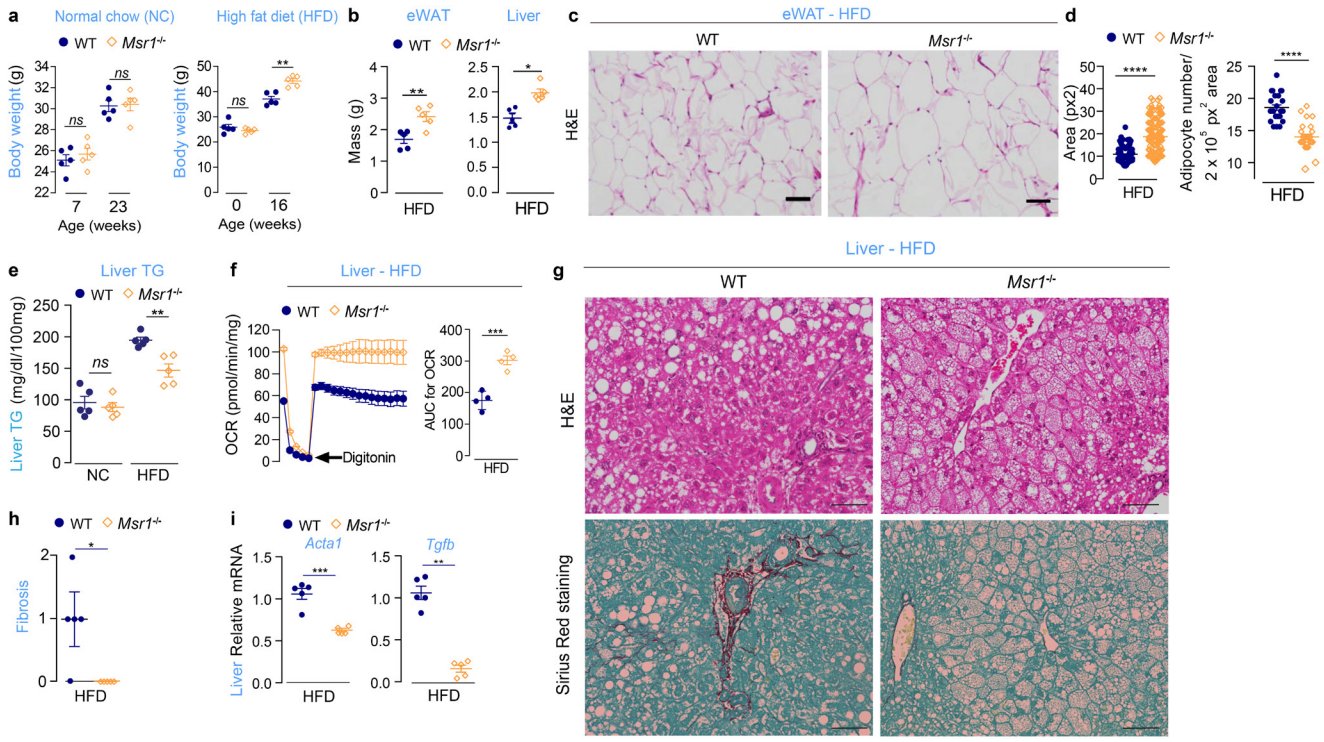

Fig. 2. Msr1 deficiency protects against HFD-associated metabolic dysregulation and liver damage. (**a**) Body weight of *Msr1*$^{+/+}$ (Wild-type, WT) and *Msr1*$^{-/-}$ male aged-matched mice fed either with normal control chow diet (NC) or high fat, high cholesterol diet (HFD) for 16 weeks (n=5 mice/experimental group). (**b**) Epididymal (eWAT) and liver mass of WT and *Msr1*$^{-/-}$ male aged-matched mice fed with HFD. (**c**) Representative images of morphology of the eWAT samples from HFD-fed WT (*Msr1*$^{+/+}$) and HFD-fed *Msr1*$^{-/-}$ aged-matched male mice, as assessed by H&E staining (n=5 mice). Scale bar 100µm. (**d**) Quantification of the adipocyte number per 2x10 px^2 area and of 100 randomly selected adipocytes per genotype in the eWAT of HFD-fed WT and HFD-fed *Msr1*$^{-/-}$ aged-matched male mice in H&E sections, (n

= 5 mice/experimental group). (**e**) Quantification of triglycerides (TG) in liver tissue samples (n = 5/experimental group). (**f**) Seahorse analysis of oxygen consumption rates (OCRs) and area under curve (AUC) of HFD-WT and HFD-fed *Msr1*$^{-/-}$ aged-matched male mice (n = 4/experimental group). (**g**) Representative images of morphology of liver samples from HFD-fed WT and *Msr1*$^{-/-}$ mice as assessed by H&E staining and Picro Sirius Red Fast Green staining (n=5 mice/experimental group). (**h**) Histopathological evaluation of liver fibrosis from HFD-fed WT and HFD-fed *Msr1*$^{-/-}$ aged-matched male mice and (**i**) qPCR analysis of selected fibrosis markers (n=5 mice/experimental group). Each symbol represent animal. Filled symbols, *Msr1*$^{+/+}$ (WT); open symbols, *Msr1*$^{-/-}$ mice. Data are presented as mean ± SEM. *p< 0.05, **p < 0.01, ***p < 0.001, ****p < 0.0001, *ns:* non-significant; unpaired Student's t-test. Scale bars 200µm.

Next we asked whether the lipid-laden environment is a proximal stimulus leading to Msr1-mediated inflammation in the liver and adipose tissue, which may explain the observed metabolic dysfunction. In agreement with our human data, histopathological analysis of the liver and adipose tissue from HFD-fed *Msr1* $^{-/-}$ mice showed no hepatic lipogranuloma and hardly any foamy macrophages compared to their WT counterparts, demonstrated by the F4/80 immunostaining (**Fig. 3a**). Triggering of Msr1 has recently been shown to induce JNK signaling pathway activation (*8*). JNK signaling is a stress-activated pathway that has been implemented in saturated fatty acid (SFA)-induced pro-inflammatory activation of macrophages (*7, 17*). Indeed, HFD-fed *Msr1*$^{-/-}$ mice exhibited reduced hepatic JNK1/2 phosphorylation compared to the WT (**Fig. S4a**). Moreover, *Msr1*$^{-/-}$ mice displayed lower IL-6 and TNF-α serum levels and reduced *Tnfa* and *Il6* gene expression in the liver and eWAT with increased mRNA levels of the anti-inflammatory gene *Adiponectin* in the eWAT (**Fig. 3b-d**) (*18*). Furthermore, *Msr1* deficiency did not reveal a reduced presence of macrophages neither in the eWAT nor in the liver but impaired pro-inflammatory macrophage activation represented by lower gene transcripts of *Tnfa* and *Il6* in isolated adipose tissue- (ATMs) and hepatic-associated macrophages (**Fig. 3e-g**). To extend these findings, we co-cultured differentiated 3T3-L1 adipocyte-like cells and lipid-fed hepatocyte-like Hepa1-6 cells indirectly with WT and *Msr1*$^{-/-}$ bone marrow-derived macrophages (BMDMs) (**Fig. S4b-d**). Consistent with the *in vivo* data, *Msr1* deficiency or the blocking of the Msr1 receptor using a monoclonal antibody attenuated pro-inflammatory response when co-cultured with adipocyte-like cells or hepatocyte-like cells compared to WT BMDMs (**Fig. S4d-f**). Altogether, these results

show that Msr1 mediates HFD-induced hepatic and adipose tissue inflammation and facilitates macrophage activation toward a pro-inflammatory phenotype.

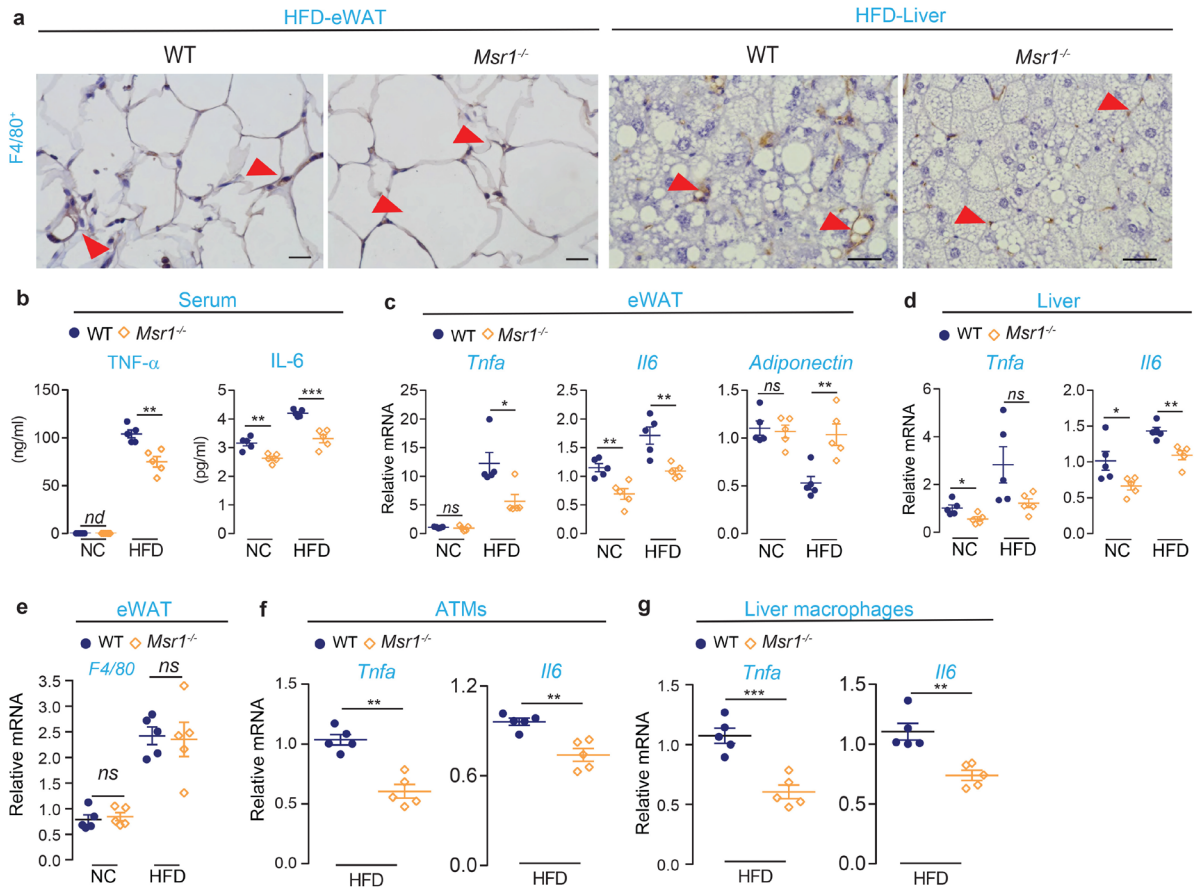

Fig. 3. Msr1 mediates HFD-induced adipose tissue and hepatic inflammation and facilitates macrophage activation toward a pro-inflammatory phenotype. (**a**) Representative images for F4/80 immunostainings in eWAT (scale bars 50µm) and liver tissue (scale bars 200µm) from HFD-fed male aged-matched WT and *Msr1*$^{-/-}$ mice (n=5/experimental group). Arrows indicate immunopositive cells showing more foamy macrophages in WT animals. (**b**) Serum levels of Tnfa and IL-6 in NC- and HFD-fed mice (n=5/experimental group). (**c-d**) Quantification of mRNA levels of *Tnfa, Il6* inflammation markers and anti-inflammatory adiponectin in the eWAT and liver of NC- and HFD-fed mice (n=5/experimental group). (**e**) The stromal vascular fraction of epididymal adipose tissue was isolated from WT and *Msr1*$^{-/-}$ mice fed with HFD (16 weeks) and examined by qPCR for *Emr1* (*F4/80*$^{+}$) gene expression of macrophages in the eWAT. (**f-g**) qPCR analysis for markers of inflammation in F4/80^{+} adipose tissue (ATMs) and liver macrophages from HFD-fed WT and *Msr1*$^{-/-}$ aged-matched male mice (n=5 mice/experimental group). Each

symbol represent animal. Filled symbols, *Msr1*$^{+/+}$ (WT); open symbols, *Msr1*$^{-/-}$ mice. Data are presented as mean ± SEM. *p< 0.05, **p < 0.01, ***p < 0.001, ****p < 0.0001, *ns*: non-significant; unpaired Student's t-test.

Next we investigated the underlying mechanism of Msr1-mediated lipid-induced inflammation. We reasoned that Msr1 is directly responsible for lipid uptake in macrophages, leading to an inflammatory response independent from other cell types. In this regard, we measured the uptake of SFA (palmitic acid) and non-SFA (nSFA, oleic acid) in BMDMs by quantifying Oil-red-O staining using confocal microscopy. The analysis revealed that Msr1 facilitates the uptake of both SFA as well as nSFA but only SFA induced enhanced levels of *Tnfa* and *Il6* transcripts and phosphorylation of JNK signalling in WT BMDMs (**Fig. 4a, Fig. S5a-c)**. Moreover, blocking of Msr1 receptor with the monoclonal antibody or the chemical inhibition of JNK signalling in macrophages abrogated the induction of *Tnfa* and *Il6* pro-inflammatory gene expression in response to SFA treatment (**Fig. 4b-d**). Next we tested whether Msr1 mediates the pro-inflammatory gene induction in response to LPS (*19*). Interestingly, *Msr1*-deficiency or the blocking of the Msr1 receptor by monoclonal antibody did not affect the pro-inflammatory response in the presence of LPS unlike SFA, showing that Msr1 facilitates lipid-induced inflammation independent of LPS (**Fig. 4e**). Moreover, mass spectrometry-based proteomics analysis of SFA-fed (12hrs) WT and *Msr1*$^{-/-}$ BMDMs showed enrichment in pathways including 'transport', 'lipid metabolic process' and 'phagocytosis' **(Fig. S5d and Table S2).** These data indicate that Msr1 regulates JNK-mediated lipid-induced pro-inflammatory activation of macrophages independent of LPS.

Several single nucleotide polymorphisms (SNPs) have been associated with susceptibility to NAFLD (*20-22*). Using a cohort of 1,483 European Caucasian patients with histologically-proven NAFLD and 17,781 European general-population controls, we identified 4 SNPs in or around the *MSR1* locus with p-values<$5*10^{-4}$, with rs41505344 as the most significant (p=1,64E-04) (**Fig. 4f** and **Table S3**). Quantitative trait analysis for rs41505344 in 430,101 patients enrolled in the UKBiobank showed a significant correlation with serum triglycerides and AST levels (**Table S4**). No effect on *MSR1* expression levels in non-diseased liver (n=151) or subcutaneous adipose tissue (n=384) was observed (**Fig. S6**). Taken together, these results suggest that genetic variations

in *MSR1* could modify the protein function and contribute to NAFLD susceptibility and obesity-related diseases or even cancer (*23*).

Here we show supporting evidence that the overflow of lipids during obesity provides a proximal signal for macrophages and induce inflammatory reaction in a MSR1-dependent manner. Macrophage scavenger receptors have been reported to play an important role in the metabolic homeostasis in adipose tissue (*14*). In this study, we demonstrate an immunoregulatory role for MSR1 in the presence of lipids, highlighting the metabolic-inflammatory axis between the liver and adipose tissue (*24, 25*). This process was shown to be independent of LPS (*19*), implementing that MSR1 is crucial in the early development of obesity-induced NAFLD.

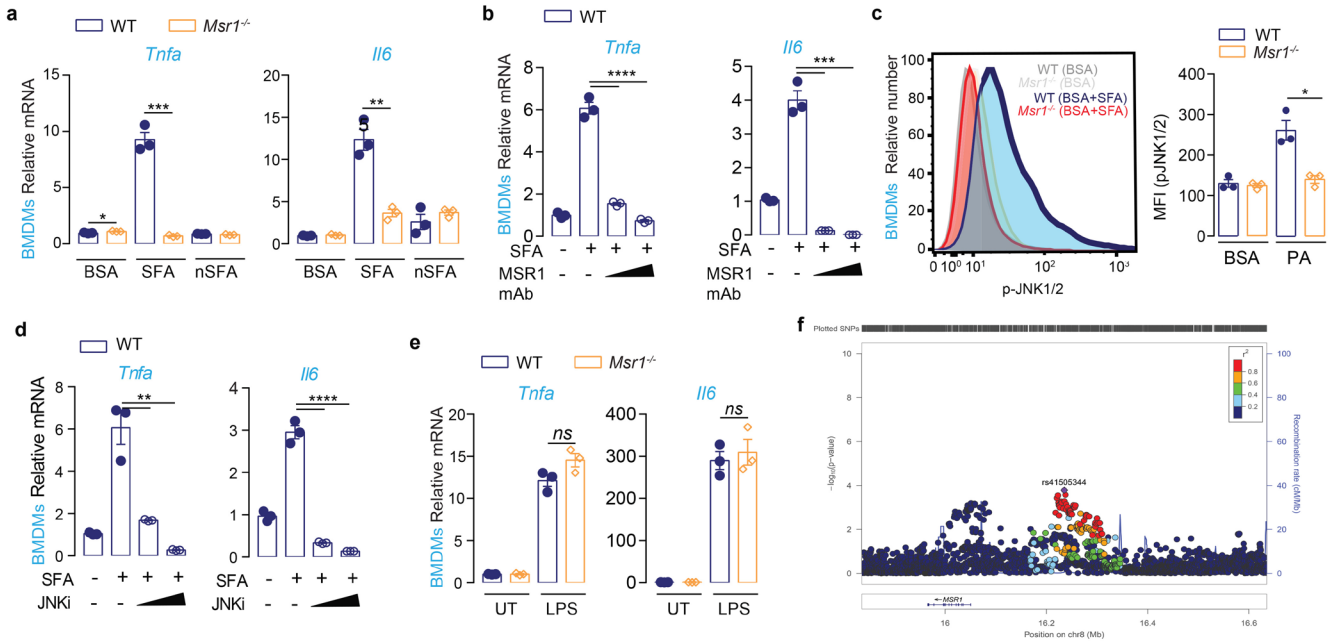

Fig. 4. Msr1 regulates lipid-induced pro-inflammatory activation of macrophages through JNK signaling independent of LPS. (**a**) qPCR analysis of *Tnfa* and *Il6* gene expression in bone marrow derived macrophages (BMDMs) isolated and differentiated from WT and *Msr1*$^{-/-}$ male aged-matched mice with or without saturated fatty acid (SFA, 1mM palmitic acid) and non-saturated fatty acid (nSFA, 2mM oleic acid) stimulation for 6 hrs. Fatty acids were coupled to fatty acid free bovine serum albumin (BSA) which was used as an unstimulated control. (**b**) qPCR analysis of *Tnfa* and *Il6* gene expression in BMDMs isolated and differentiated from WT with or without SFA (1mM palmitic acid) stimulation that were pre-treated with 10 or 25µg/ml anti-Msr1 monoclonal antibody (2F8) for 6 hrs. (**c**) Flow cytometry analysis and quantification of JNK1/2 phosphorylation in WT and *Msr1*$^{-/-}$ BMDMs stimulated with SFA (1 mM palmitic acid PA). BSA was used as an unstimulated control. (**d**) qPCR analysis of *Tnfa* and *Il6* gene expression in

BMDMs isolated and differentiated from WT aged-matched male mice with or without SFA (1mM palmitic acid) stimulation for 6 hrs that were pre-treated with 1 or 3 μM JNK inhibitor for 1hr. (**e**) qPCR analysis of *Tnfa* and *Il6* gene expression in WT and *Msr1*$^{-/-}$ BMDMs cells stimulated with or without 100 ng/ml of ultra-pure lipopolysaccharide (LPS) for 3 hrs. (**f**) Locus plot showing *MSR1* rs41505344 SNP based on case-control analysis comparing 1,483 histologically characterised NAFLD samples with 17,781 matched population controls. qPCR and flow cytometry data are shown as mean ± SEM. $^{***}p < 0.001$, $^{****}p < 0.0001$, *ns*: non-significant; unpaired Student's t-test.

Materials and Methods

Patient selection

For the histopathological and nanoString® study, 214 liver and adipose tissue samples from Caucasian patients were included. 184 formalin-fixed paraffin-embedded (FFPE) or frozen liver biopsies samples were obtained from patients diagnosed with histological proven NAFLD at the Freeman Hospital, Newcastle Hospitals NHS Foundation Trust, Newcastle-upon-Tyne, UK and at the Pitié-Salpêtrière Hospital, Paris, France. In addition 20 FFPE subcutaneous adipose tissue samples and 10 matching omental adipose tissue samples were obtained from obese patients with or without NALFD, diagnosed and treated at the Pitié-Salpêtrière Hospital, Paris, France. For the Genome Wide Association Study (GWAS), 1,483 patients with histological proven NAFLD were included recruited at different European centers (the Freeman Hospital, Newcastle Hospitals NHS Trust Foundation, Newcastle upon Tyne, UK; Addenbrooke's Hospital, Cambridge, UK; Nottingham University Hospitals NHS Trust, Nottingham, UK; Inselspital Hospital, Bern, Switzerland; Antwerp University Hospital, Belgium; Pitié-Salpêtrière Hospital, Paris, France; University Hospital, Linköping, Sweden, Oskarshamn County Hospital, Sweden; University Medical Center, Mainz, Germany; Città della Salute e della Scienza di Torino Hospital, Turin, Italy; Section of Gastroenterology and Hepatology, University of Palermo, Italy.). All liver tissue samples for the histopathological and nanoString® study and 78% of the GWAS samples were centrally scored according to the semiquantitative NASH-CRN Scoring System (NAS) (*1*) by two expert liver pathologists (DT & PB). Fibrosis was staged from F0 through to F4 (cirrhosis). Alternate diagnoses and etiologies were excluded, including excessive alcohol intake, viral hepatitis, autoimmune liver diseases and steatogenic medication use. This study was approved by the relevant Ethical Committees in the participating countries.

nanoString®

mRNA was isolated from frozen tissue samples using the Allprep DNA/RNA Micro kit (Qiagen) or from FFPE samples using the High Pure FFPET RNA Isolation Kit (06650775001, Life Science Roche). Custom-made assay panels were run on the nanoString® nCounter analysis system (nanoString®). The nSolver 3.0 software (nanoString®) was used for positive and negative control probe validation and the data were normalized to three housekeeping genes (*RPL19*, *SRSF4* and *YWHAZ*).

Immunohistochemistry of human patient samples

Human FFPE tissue samples (NAFLD liver biospies n=14, subcutaneous/omental adipose tissue samples n=30) were immunostained with mouse monoclonal antibody directed against human Macrophage Scavenger Receptor 1 (MSR1, aa197-451, clone OTI9E5, LS-C336674; LSBio; EDTA, 1/50). In addition, the liver biopsies were immunostained with monoclonal mouse anti-human CD68 antibody (clone KP1; Dako; EDTA, ready-to-use). Envision Flex+ reagent (Dako) was used as secondary antibody at room temperature and 3',3'-diaminobenzidine for the visualization step. Immunopositive cells in the liver biopsies were quantified in the parenchyma and the portal tract as previously reported (*2*).

Animals

Msr1$^{-/-}$ mice were kindly provided by Prof. Siamon Gordon, University of Oxford. All mice were maintained under specific pathogen free conditions and experiments were approved by the Institutional Animal Care and Use Committee. Mice had free access to water and were fed either standard chow or high-fat and high-cholesterol diets (45%-HFD; 820263,Special Diet Services) ad libitum. Body weight was measured weekly during the feeding period and compared with liver weight and visceral fat mass after the animals were sacrificed. On the day prior to sacrifice, the mice were subjected to overnight fasting.

Glucose tolerance test (GTT)

To assess glucose tolerance, 8-week-old mice were fed a standard chow or a 45% high-fat diet for 16 weeks. Mice were injected intraperitoneally with 2 g glucose/kg body weight after overnight

fasting for GTT assay. Tail-blood glucose levels were measured by using an ACCU-CHEK Aviva (Roche) glucometer.

Bioenergetics

Tissue bioenergetics was determined using a Seahorse respirometer as previously described (15). Briefly, WAT and liver were collected rapidly after sacrifice, and rinsed with Krebs-Henseleit buffer (KHB) (111mM NaCl, 4.7mM KCl, 2mM MgSO4, 1.2mM Na2HPO4, 0.5mM carnitine, 2.5mM glucose and 10mM sodium pyruvate). Tissues were cut into small pieces (6-10mg) and quickly transferred to individual wells of a XF24 plate. Individual pieces were stabilized from excessive movement by isletcapture screens (Seahorse Bioscience), and 450µL KHB was added to each well. Digitonin was added to enhance plasma membrane permeability. Basal oxygen consumption rates (OCR) were determined according to the following plan: Basal readings recorded every 2min for 10 readings, followed by exposure to digitonin. Subsequent readings were recorded after 2min mixing and 2min rest. Basal OCR values were normalized to individual tissue weights.

Blood biochemical analysis

Blood samples were obtained from the heart by cardiac puncture, and serum samples were preserved at −80 °C for biochemical analyses as described below. The total triglycerides (TG), free fatty acids (FFA) levels were determined using the fluorometric method using the commercial available kit from Abcam (ab178780) and (ab65341). The serum Leptin was measured using an ELISA (Quantikine, RD systems). The serum TNF-□ and IL-6 were measured using an ELISA (DuoSet Elisa, RD systems).

Assessments of hepatic TGs and eWAT FAs

The liver TG and eWAT fatty acids concentrations were determined using the fluorometric method using the commercial available kit from Abcam (ab178780) and (ab65341).

Immunohistochemistry and analysis of mouse tissue sections

Histology was performed on WAT and liver following fixation in 10% formalin for 24 hr, dehydration, and embedding in paraffin. Sections (5 µm) were cut and stained using hematoxylin

and eosin (H&E). Mouse tissue samples were immunostained with rat monoclonal anti-F4/80 antibody (ab6640; Abcam, Cambridge, UK; citrate 1/50) and a Goat Anti-Rat IgG H&L (ab97057; Abcam; 1/100), followed by 3',3'-diaminobenzidine for the visualization. Histopathological scoring of the liver samples was based on the semiquantitative NASH-CRN Scoring System (NAS). In addition, sinusoidal fibrosis was scored as 0=absent, 1=mild, 2=moderate, 3=prominent. Cell size of the adipose tissue was quantified based on a haematoxylin & eosin staining using Nikon NIS elements software.

Adipose-tissue and liver-associated macrophages isolations

Digested epididymal fat pads and liver passed through either a 100-µm or 70--µm filters (BD, falcon) and spun at 300*g* for 5 min. Thereafter, adipose tissue macrophages were enriched using magnetic immunoaffinity isolation with anti- F4/80^{+} antibodies conjugated to magnetic beads (MACS; Miltenyi Biotec, Auburn, CA) and the liver associated macrophages were obtained by the isotonic 33% Percoll (Sigma-Aldrich) solution method.

Cell culture and stimulation

Mus musculus hepatoma cell line Hepa 1-6 [Hepa1-6] (ATCC® CRL-1830™) were maintained in Dulbecco's Modified Eagle's Medium (DMEM) (Gibco, Life Technologies) containing 10% (v/v) Fetal Calf Serum (FCS, Gibco, Life Technologies) and 1% Penicilin-Streptomycin (Gibco, Life Technologies). 3T3-L1 pre-adipocytes were differentiated through 72 hours incubation with 0.5 nM 3-isobuty1 methylxanthine (IBMX), 1 µM dexamethasone and 10 µg/ml insulin, followed by 48 hours incubation with 2 µg/ml insulin. Cells were subsequently cultured in Dulbecco's Modified Eagle's Medium (DMEM) with 25 mM glucose and 10% calf serum for an additional 21 days, which allowed complete differentiation and hypertrophy to develop. Bone-marrow-derived macrophages (BMDMs) were generated by culturing the mouse bone marrow cells in IMDM medium (GIBCO, Life Technologies) supplemented with 10% FCS (GIBCO, Life Technologies), 100 U/ml penicillin (Gibco, Life Technologies), and 100 g/ml streptomycin (Gibco,LifeTechnologies), 2 mM glutamine (Glutamax, Gibco, Life Technologies) and 15% (v/v) L929 conditional medium. BMDMs were either stimulated with LPS (100 ng/ml, Invivogen) or lipids. *In vitro* lipid loading was performed using a 1% fatty-acid depleted Bovine Serum Albumin (BSA, Sigma Aldrich) vehicle or either with 1mM palmitic acid or 2mM oleic acid (Sigma-

Aldrich) conjugated to fatty acid-depleted BSA for 6, 12h or 24 hrs. Cells were fixed with 10% formaldehyde for 10 min and stained with a 60% Oil Red O/isopropanol solution (Sigma-Aldrich). The slides were analyzed using the Leica TCS SP8 confocal microscope platform (Leica Biosystems).

Immunoblot analysis

Liver lysates were separated by SDS-PAGE and transferred to Immobilon-P PVDF membranes (Millipore). After blocking with 5% nonfat dry milk in Tris-buffered saline and 0.1% Tween (TBS-T), the membranes were incubated with the indicated antibodies overnight at 4°C. After 2hr incubation with the appropriate horseradish peroxidase-conjugated antibodies, the immune complexes were detected by chemiluminescence (Thermo Scientific).

Quantitative Real-time PCR analysis

Tissue samples were in TRIzol. RNA was isolated using RNeasy kit from Qiagen. Total RNA (500–1,000 ng) was used to synthesize cDNA with the QuantiTect Reverse Transcription Kit (Qiagen). Quantitative real-time PCR analysis was performed using the Applied Biosystem SYBR Green Mastermix and analysed using either the StepOne Plus or Applied Biosystems 7500 Fast Real-Time PCR systems. The results were normalized to *Tbp* and expressed as fold change relative to RNA samples from control or mock-treated cells using the comparative CT method ($\Delta\Delta C_T$). The following validated QuantiTect primer assays (Qiagen) were used: *Tnfa and Il6.*

Primer name	*Forward*	*Reverse*
Tbp	*(f) 5'-gaagctgcggtacaattccag-3'*	*(r) 5'-ccccttgtacccttcaccaat-3'*
Acta1	*(f) 5'-cccaaagctaaccgggacaa-3'*	*(r) 5'-ccagaatccaacacgatgcc-3'*
Tgfb	*(f) 5'-agaccacatcagcattgagtg-3'*	*(r) 5'-ggtggcaacgaatgtagctgt-3'*
Adiponectin	*(f) 5'-ggagtgttcgtgggcttagg-3'*	*(r) 5'-gcacgtccggtgatatagagg-3'*
Leptin	*(f) 5'atgtgcccttccgatatacaacc-3'*	*(r) 5'-cgtgtcatccactaatcttctgg-3'*
F4/80 (Emr1)	*(f) 5'-ctttggctatgggcttccagtc-3'*	*(r) 5'-gcaaggaggacagagtttatcgtg -3'*

Flow cytometry

Following treatment, WT and *Msr1*$^{-/-}$ BMDMs were stained with FcBlock (BD) followed by pJNK1/2 (#5755, Cell Signaling) staining according to manufacturer's protocol and analysed using a BD Facs Canto cytometer (BD Biosciences). Data were processed using FlowJo Software v10.

Mass spectrometry analysis

Following treatment, total cell lysate of WT and Msr1-/- BMDMs were lysed in 5% SDS, 50 mM TEAB pH 7.55 (S-Trap), sonicated and protein quantification was determined using the BCA Protein Assay Kit (Pierce Protein). Each sample was reduced by adding TCEP to a final concentration of 10 mM for 30 min at room temperature followed by alkylation with10 mM iodoacetamide for 30 min in the dark followed by S-trap digestion. Briefly, samples were acidified by addition of 2.5µL of 12% phosphoric acid and diluted with 165 µL of S-trap binding buffer; 90% MeOH, 100mM TEAB, pH 7.1. The acidified samples were then loaded onto the S-trap spin column and centrifuged for 1 minute at 4000 xg. Columns were washed five times with s-trap binding buffer before addition of porcine trypsin (1:20) (Pierce) in 25 µL of 50 mM TEAB to the column. Samples were incubated at 47 °C for 2 hours. Peptides were eluted by washing the column with firstly 50 mM TEAB, pH 8.0 (40 µL), followed by 0.2% FA (40 µL) and finally 0.2% FA, 50% CAN (40 µL). Peptides were then dried under vacuum.

Label-free mass spectrometry acquisition

Peptide samples were separated on an Ultimate 3000 RSLC system (Thermo Scientific) with a C18 PepMap, serving as a trapping column (2 cm x 100 µm ID, PepMap C18, 5 µm particles, 100 Å pore size) followed by a 50 cm EASY-Spray column (50 cm x 75 µm ID, PepMap C18, 2 µm particles, 100 Åpore size) (Thermo Scientific). Buffer A contained 0.1% FA and Buffer B 80% ACN, 0.1% FA. Peptideswere separated with a linear gradient of 1-35% (Buffer B) over 120 minutes followed by a step from 35-90% ACN, 0.1% FA in 0.5 minutes at 300 nL/min and held at 90% for 4 minutes. The gradient wasthen decreased to 1% Buffer B in 0.5 minutes at 300 nL/min for 10 minutes. Mass spectrometric identification was performed on an Orbitrap QE HF mass spectrometer (Thermo Scientific) operated "Top Speed" data dependant mode in positive ion mode. FullScan spectra were acquired in a range from 400 m/z to 1500 m/z, at a resolution of 120 000 (at 200 m/z), with an automated gain control (AGC) of 1,000,000 and a maximum injection

time of 50 ms. Charge state screening is enabled to exclude precursors with a charge state of 1. For MS/MS fragmentation, the minimum AGC was set to 5000 and the most intense precursor ions were isolated with a quadrupole mass filter width of 1.6 m/z and 0.5 m/z offset. Precursors were subjected to CID fragmentation that was performed in one-step collision energy of 25%. MS/MS fragments ions were analysed in the Orbitrap mass analyser with a 15 000 resolution at 200 m/z.

Mass spectrometry data analysis

Protein identification and label free quantification was performed using MaxQuant Version 1.5.8.3. Trypsin/P set as enzyme; stable modification carbamidomethyl (C); variable modifications Oxidation (M), Acetyl (Protein N-term), Deamidation (NQ), Gln & Glu to pyro-Glu; maximum 8 modifications per peptide, and 2 missed cleavage. Searches were conducted using a Uniprot human database downloaded July 12, 2017 plus common contaminants. Identifications were filtered at a 1% FDR at the peptide level, accepting a minimum peptide length of 5. Quantification was performed using razor and unique peptides, and required a minimum count of 2. "Re-quantify" and "match between runs" were enabled. LFQ intensities were extracted for each protein/condition and used for downstream analyses. Statistical analyses were performed in Perseus (v1.6.6.0). T-test-based statistics were applied on LFQ intensity values to extract the significant regulated proteins. DAVID annotation tool was used for pathway enrichment.(*3, 4*) Data were visualized with GOPlot 1.0.2.(*5*)

GWAS analysis

Genotyping was performed using the Illumina OmniExpressExome BeadChip as reported elsewhere. SNP imputation in the 1,483 European NAFLD cases was carried out using the Michigan Imputation Server (https://imputationserver.sph.umich.edu/start.html#!pages/home).(*6*) Selected European ancestry controls (n=17,781) were obtained from Wellcome Trust Case Control Consortium, the Hypergenes cohort (http://www.hypergenes.eu/dissemination.html#pub), KORA (https://epi.helmholtz-muenchen.de/), and Understanding Societies (https://www.understandingsociety.ac.uk/).

Expression quantitative trait loci

The UK Biobank (https://www.ukbiobank.ac.uk/) is a large population based study comprising more than 500,000 adult individuals (aged between 40-69 years at recruitment) who visited 22 recruitment centers throughout the United Kingdom between 2006 and 2014. Both the phenotypic and genotypic data used in the present study were obtained from the UK Biobank under Application Number 37142. The UK Biobank study received ethical approval from the National Research Ethics Service Committee North West Multi-Centre Haydock (reference 16/NW/0274) (*7, 8*). For the present study, we restricted our analysis to a subset of UK Biobank participants with European ancestry by adding individuals who self-reported as being 'Irish' or 'Any other white background' (after removal of outliers based on first 2 genetic principal components) to the subset of white British ancestry(*7, 9*). We then excluded individuals with (1) excessive relatives (more than 10 putative third-degree relatives); (2) a mismatch between the self-reported and genetically inferred gender; or (3) putative sex chromosome aneuploidy and (4) those identified by the UK Biobank as outliers based on heterozygosity and missingness (*10-12*). We used main and secondary (UK Biobank data-fields 41202 and 41204) ICD10 diagnoses to define "chronic liver disease" by merging the codes K70.0-K70.4, K70.9, K72.1, K73.0-K73.2, K73.8, K73.9, K74.0-K74.2, K74.4, K74.6, K76.0, K76.6, K76.7-K76.9 and I85. Similarly, "all-cause liver cirrhosis" was defined by merging the following ICD10 codes: K70.2-K70.4, K74.0-K74.2, K74.6, K76.6 (Portal hypertension), or I85 (*13*). Details of the genotyping and imputation procedures in the UK Biobank have been previously described(*7*). Briefly, UK Biobank participants were genotyped using two similar arrays: the UK BiLEVE or UK Biobank Axiom array. Genotyped data were then imputed based on the 1000 Genomes Phase 3, UK10K haplotype, and Haplotype Reference Consortium (HRC) reference panels (*7*). For *MSR1* rs41505344, we used UKB version 3 of imputed genotype data (info score = 0.98) and converted imputed genotype probabilities to hard genotype calls using PLINK 2 (*14*). The associations between liver cirrhosis and *MSR1* rs41505344 was examined using binary logistic regression adjusted for age, gender, BMI, the first ten genomic principal components, the array type and the assessment center. Continuous traits were first rank-based inverse normal transformed, and their association with rs41505344 was then examined using linear regression adjusted for the abovementioned covariates. All analyses were performed under an additive genetic model.

eQTL in normal tissue was performed on data obtained from 151 human liver and 384 adipose tissue samples using the GTEx portal (https://gtexportal.org/).

Statistical analysis

All data are shown as mean ± SEM. Shapiro-Wilk test was used to test normality. Statistical analysis was performed using Mann-Whitney U test, unpaired two-tailed Student's T-test, analysis of variance (ANOVA), Spearman's rho correlation were using GraphPad Prism 8.0.1 (GraphPad Software Inc., San Diego, California, USA).

Reagents and antibodies

Free-fatty acid bovine serum albumin (BSA), palimitic acid, oleic acid, carnitine, glucose, digitonin, Percoll, 3-isobuty1 methylxanthine dexamethasone, insulin and Oil-red-O-staining were from Sigma-Aldrich. Collagenase was purchased from Roche, DNAse I from Thermo Scientific. Ultrapure lipopolysaccharide (LPS) was purchased from Invivogen. The following antibodies were purchased from Cell Signaling Technology: p-JNK (#9251) and p-JNK PE conjugate (#5755). Antibodies purchased from Abcam were as follows: F4/80 (#ab6640), Goat Anti-Rat IgG H&L (#ab97057), Msr1 (#ab151707), b-Tubulin (#ab6046). The antibody used for MSR1 immunohistochemistry was clone OTI9E5 (from LSBio, # LS-C336674). Horse radish peroxidase (HRP)-conjugated anti-mouse and anti-rabbit were from Thermo Scientific.

References

1. Q. M. Anstee, H. L. Reeves, E. Kotsiliti, O. Govaere, M. Heikenwalder, From NASH to HCC: current concepts and future challenges. *Nat Rev Gastroenterol Hepatol*, (2019).
2. Z. M. Younossi *et al.*, Global epidemiology of nonalcoholic fatty liver disease-Meta-analytic assessment of prevalence, incidence, and outcomes. *Hepatology* **64**, 73-84 (2016).
3. C. A. Moylan *et al.*, Hepatic gene expression profiles differentiate presymptomatic patients with mild versus severe nonalcoholic fatty liver disease. *Hepatology* **59**, 471-482 (2014).
4. K. Kazankov *et al.*, The role of macrophages in nonalcoholic fatty liver disease and nonalcoholic steatohepatitis. *Nat Rev Gastroenterol Hepatol* **16**, 145-159 (2019).
5. A. Leroux *et al.*, Toxic lipids stored by Kupffer cells correlates with their pro-inflammatory phenotype at an early stage of steatohepatitis. *J Hepatol* **57**, 141-149 (2012).
6. P. Ramachandran *et al.*, Resolving the fibrotic niche of human liver cirrhosis at single-cell level. *Nature*, (2019).
7. G. I. Lancaster *et al.*, Evidence that TLR4 Is Not a Receptor for Saturated Fatty Acids but Mediates Lipid-Induced Inflammation by Reprogramming Macrophage Metabolism. *Cell Metab* **27**, 1096-1110 e1095 (2018).
8. M. Guo *et al.*, Triggering MSR1 promotes JNK-mediated inflammation in IL-4-activated macrophages. *EMBO J* **38**, (2019).
9. J. J. Manning-Tobin *et al.*, Loss of SR-A and CD36 activity reduces atherosclerotic lesion complexity without abrogating foam cell formation in hyperlipidemic mice. *Arterioscler Thromb Vasc Biol* **29**, 19-26 (2009).
10. M. Van Eck *et al.*, Effect of human scavenger receptor class A overexpression in bone marrow-derived cells on cholesterol levels and atherosclerosis in ApoE-deficient mice. *Arterioscl Throm Vas* **20**, 2600-2606 (2000).
11. S. McPherson *et al.*, Evidence of NAFLD progression from steatosis to fibrosing-steatohepatitis using paired biopsies: implications for prognosis and clinical management. *J Hepatol* **62**, 1148-1155 (2015).

12. O. Krenkel *et al.*, Therapeutic Inhibition of Inflammatory Monocyte Recruitment Reduces Steatohepatitis and Liver Fibrosis. *Hepatology*, (2017).
13. O. Govaere *et al.*, High-throughput sequencing identifies aetiology-dependent differences in ductular reaction in human chronic liver disease. *J Pathol* **248**, 66-76 (2019).
14. D. A. Jaitin *et al.*, Lipid-Associated Macrophages Control Metabolic Homeostasis in a Trem2-Dependent Manner. *Cell* **178**, 686-698 e614 (2019).
15. N. Martinez-Lopez *et al.*, Autophagy in the CNS and Periphery Coordinate Lipophagy and Lipolysis in the Brown Adipose Tissue and Liver. *Cell Metab* **23**, 113-127 (2016).
16. G. Farrell *et al.*, Mouse Models of Nonalcoholic Steatohepatitis: Toward Optimization of Their Relevance to Human Nonalcoholic Steatohepatitis. *Hepatology* **69**, 2241-2257 (2019).
17. M. Cao *et al.*, c-Jun N-terminal kinases differentially regulate TNF- and TLRs-mediated necroptosis through their kinase-dependent and -independent activities. *Cell Death Dis* **9**, 1140 (2018).
18. N. Ouchi, K. Walsh, Adiponectin as an anti-inflammatory factor. *Clin Chim Acta* **380**, 24-30 (2007).
19. E. Gabele *et al.*, DSS induced colitis increases portal LPS levels and enhances hepatic inflammation and fibrogenesis in experimental NASH. *J Hepatol* **55**, 1391-1399 (2011).
20. S. Romeo *et al.*, Genetic variation in PNPLA3 confers susceptibility to nonalcoholic fatty liver disease. *Nat Genet* **40**, 1461-1465 (2008).
21. J. Kozlitina *et al.*, Exome-wide association study identifies a TM6SF2 variant that confers susceptibility to nonalcoholic fatty liver disease. *Nat Genet* **46**, 352-356 (2014).
22. Y. L. Liu *et al.*, TM6SF2 rs58542926 influences hepatic fibrosis progression in patients with non-alcoholic fatty liver disease. *Nat Commun* **5**, 4309 (2014).
23. J. Xu *et al.*, Germline mutations and sequence variants of the macrophage scavenger receptor 1 gene are associated with prostate cancer risk. *Nat Genet* **32**, 321-325 (2002).
24. D. S. Ghorpade *et al.*, Hepatocyte-secreted DPP4 in obesity promotes adipose inflammation and insulin resistance. *Nature* **555**, 673-677 (2018).
25. C. Rosso *et al.*, Crosstalk between adipose tissue insulin resistance and liver macrophages in non-alcoholic fatty liver disease. *J Hepatol* **71**, 1012-1021 (2019).

Acknowledgments

The authors would like to thank the Newcastle NanoString Core Facility and Newcastle Molecular Pathology Node Proximity Laboratory for their technical support and the members of AH's group for the critical reading of the manuscript.

Funding

This study has been supported by the EPoS (Elucidating Pathways of Steatohepatitis) consortium funded by the Horizon 2020 Framework Program of the European Union under Grant Agreement 634413 and the Newcastle NIHR Biomedical Research Centre (to QMA), the Newcastle University start-up funding and the Wellcome Trust Investigator Award (215542/Z/19/Z) (to MT), Knut och Alice Wallenberg Foundation Wallenberg Centre for molecular and translational medicine, University of Gothenburg, Sweden and Åke Wirbergs Research funding #M18-0121 (to AH), and Rosetrees Trust (to NML).

Author contributions

AH and OG conceived the study. Study design, manuscript drafting and funding: AH, OG, MT and QMA. Manuscript preparation: AH, OG, MT, QMA and SKP. *In vivo* experiments: AH and NML. *In vitro* experiments: AH, OG and SKP. Histopathology: OG and DT. Nanostring analysis: OG. Mass spectrometry-based analysis: AH, JP and MT. GWAS analysis: RD, HJC, AKD. eQTL UKBiobank data: RMM, OJ, SR. All authors contributed to data collection and interpretation, and critically revised the manuscript.

Competing interests

The authors disclose no conflicts.

Supplementary Figures

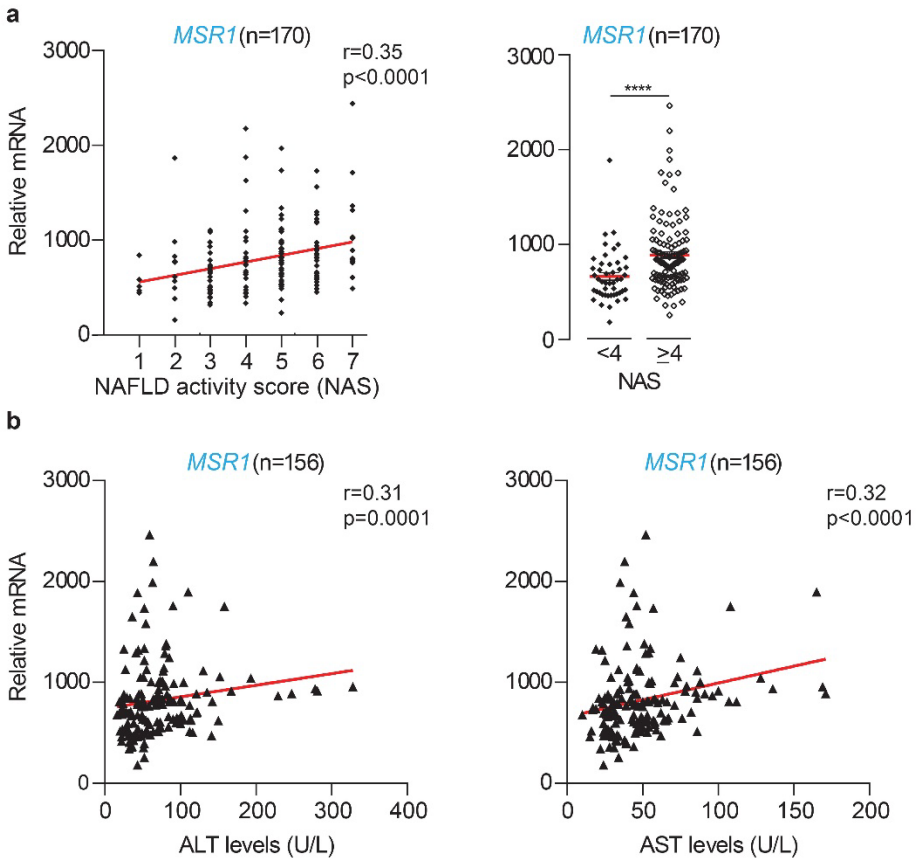

Fig. S1. Macrophage Scavenger Receptor 1 (MSR1) expression in human non-alcoholic fatty liver disease (NAFLD). *MSR1* expression based nanoString® in patients with non-alcoholic fatty liver (n=170). (**a**) Correlation of *MSR1* gene expression with the NAFLD activity score (NAS; Spearman r=0.34, p<0.0001) which represents the sum of steatosis grading, lobular inflammation and ballooning. Patients stratified based on NAS show higher *MSR1* expression (Data are presented as mean ± SEM, Mann-Whitney-U test, **** p<0.0001). (**b**) Correlation of *MSR1* mRNA levels with clinicopathological features including ALT (n=156, Spearman r=0.31, p=0.0001) and AST levels (n=156, Spearman r=0.32, p<0.0001).

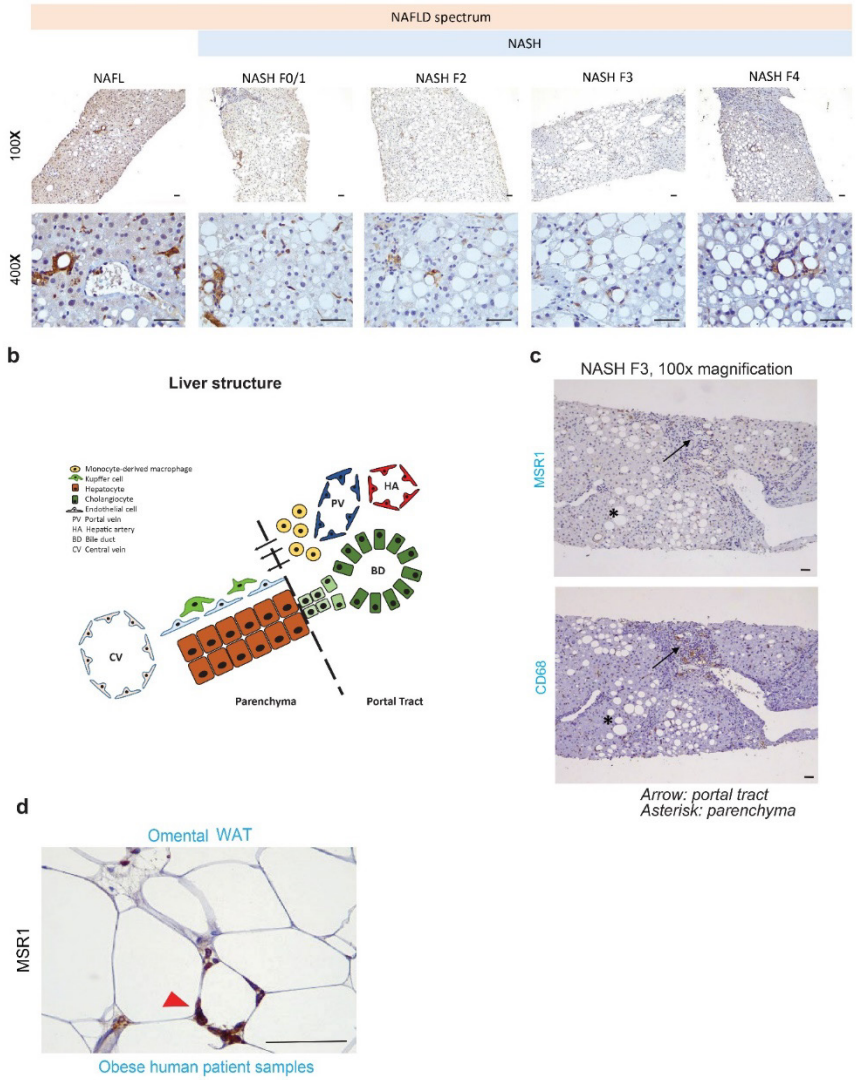

Fig. S2. Immunohistochemistry for MSR1 and CD68 in human non-alcoholic fatty liver disease (NAFLD). (**a**) Representative images of the MSR1 immunostainings in the spectrum of NAFLD going from non-alcoholic fatty liver (NAFL) to non-alcoholic steatohepatitis (NASH) with fibrosis stages ranging from F0/1 to F4. (**b**) Schematic overview displaying resident and infiltrating macrophages. (**c**) Representative images of MSR1 and CD68 immunostainings in a NASH F3 patient liver biopsy indicating the differences between parenchymal (asterisk) and portal positivity (arrow). (**d**) Immunohistochemistry showing MSR1 expression in omental adipose tissue from a human obese patient. Red arrow indicates MSR1 immunopositive cells and crown-like structure within adipose tissue. Scale bar 100µm.

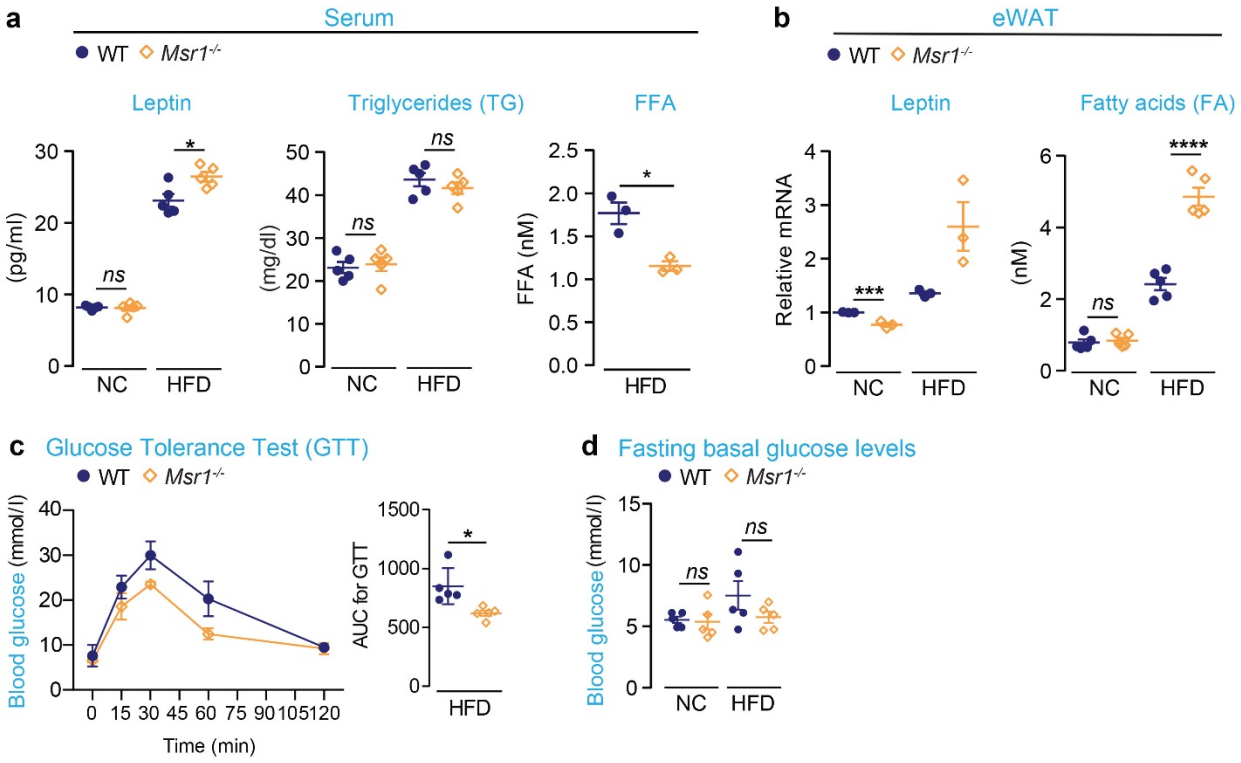

Fig. S3. Msr1 deficiency promotes adiposity and improves glucose uptake. (**a**) Serum leptin, triglycerides (TGs) and free fatty acids (FFAs) levels of NC- and HFD-fed WT and *Msr1*$^{-/-}$ male aged-matched mice. (**b**) Quantification of mRNA *leptin* levels and enumeration of fatty acid content in the eWAT of NC- and HFD-fed WT and *Msr1*$^{-/-}$ mice. (**c**) Glucose tolerance test on overnight fasted mice treated by i.p. injection with glucose during the 15th week of HFD feeding; AUC (area under curve) of HFD-WT and *Msr1*$^{-/-}$ male aged-matched mice (**d**) Basal blood glucose levels of fasted overnight HFD-WT and *Msr1*$^{-/-}$ male aged-matched mice. Each symbol represents one animal. Filled symbols, WT (*Msr1*$^{+/+}$); open symbols, Msr1$^{-/-}$ mice; (n=5 mice/experimental group). Data are presented as mean ± SEM. *p< 0.05, **p < 0.01, ***p < 0.001, ****p < 0.0001, *ns:* non-significant; unpaired Student's t-test.

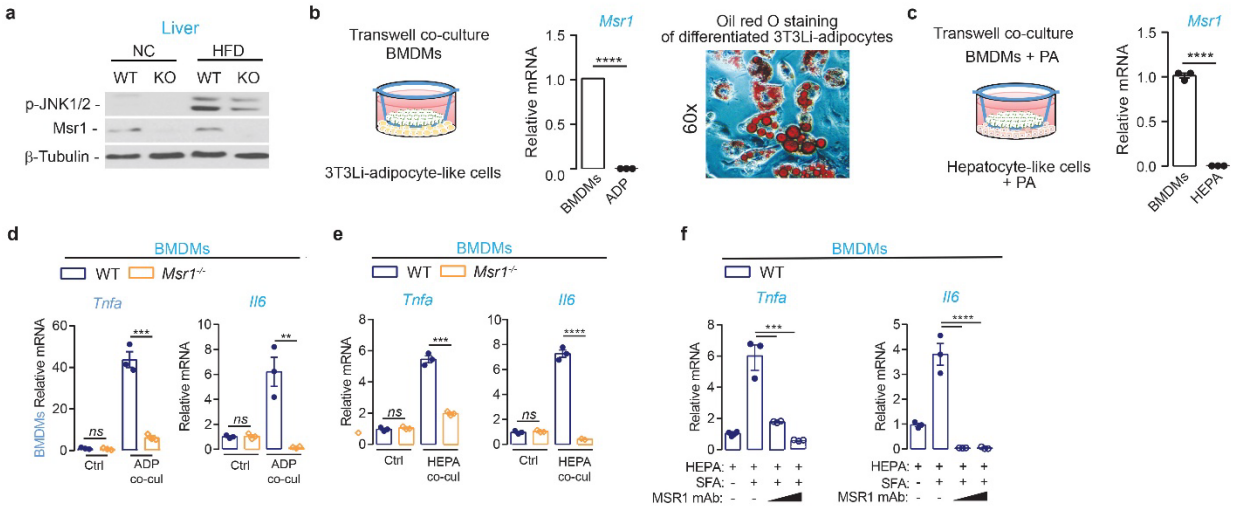

Fig. S4. The co-cultures of WT and Msr1$^{-/-}$ BMDMs with adipocyte- and hepatocyte-like cells. (**a**) Western blotting analysis of p-JNK1/2 in the liver lysates isolated from male aged-matched WT and *Msr1*$^{-/-}$mice fed either with NC or HFD for 16 weeks. (**b-c**) Scheme depicts transwell co-culture of BMDMs from WT or *Msr1*$^{-/-}$ male aged-matched mice with either (**b**) 3T3-L1 adipocytes or (**c**) Hepa1-6 cells. (**b**) Oil-red-O-staning of differentiated of 3T3-L1 adipocytes. qPCR analysis of *Msr1* in BMDMs and 3T3-L1 adipocytes (ADP) and Hepa1-6 cells (HEPA). (**d**) qPCR analysis of *Tnfa* and *Il6* gene expression in BMDMs isolated and differentiated from WT and *Msr1*$^{-/-}$ mice, comparing bare BMDMs with BMDMs co-cultured indirectly in the transwell system with 3T3-L1 adipocyte-like cells (ADP co-cul). (**e**) qPCR analysis of *Tnfa* and *Il6* gene expression in BMDMs isolated and differentiated from WT and *Msr1*$^{-/-}$ mice, comparing bare BMDMs with BMDMs co-cultured indirectly in the transwell system with saturated fatty acid-treated (SFA, 1 mM palmitic acid, 12 hrs) Hepa1-6 cells (HEPA co-cul). Fatty acids were coupled to BSA fatty acids free, BSA was used as an unstimulated control. (**f**) qRT-PCR analysis of *Tnfa* and *Il6* gene expression in BMDMs isolated and differentiated from WT mice pre-treated with 0, 12.5, 25µg/ml of anti-Msr1 monoclonal antibody (2F8) for 1 h followed by indirect co-culture in the transwell system with SFA-treated Hepa1-6 cells (1 mM palmitic acid, 12 hrs). Data are presented as mean ± SEM. *p< 0.05, **p < 0.01, ***p < 0.001, ****p < 0.0001, *ns:* non-significant; unpaired Student's t-test.

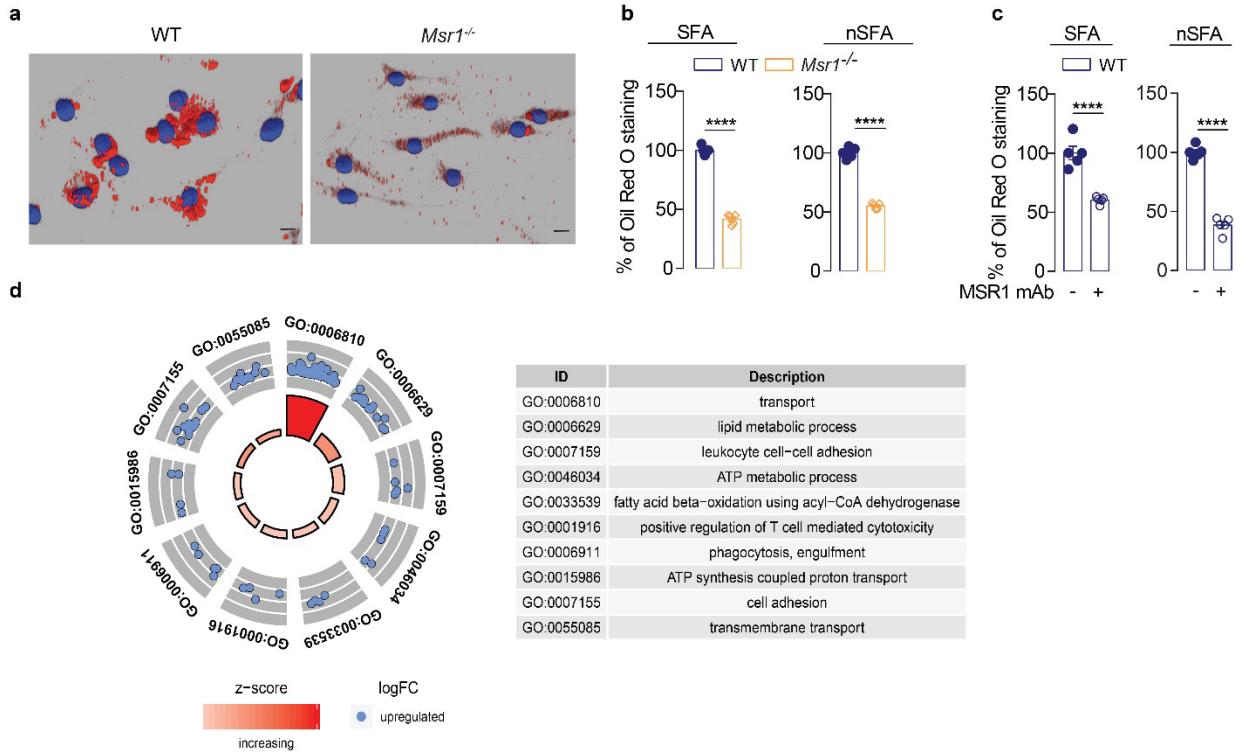

ID	Description
GO:0006810	transport
GO:0006629	lipid metabolic process
GO:0007159	leukocyte cell−cell adhesion
GO:0046034	ATP metabolic process
GO:0033539	fatty acid beta−oxidation using acyl−CoA dehydrogenase
GO:0001916	positive regulation of T cell mediated cytotoxicity
GO:0006911	phagocytosis, engulfment
GO:0015986	ATP synthesis coupled proton transport
GO:0007155	cell adhesion
GO:0055085	transmembrane transport

Fig. S5. Msr1 mediates lipid uptake and lipid processing pathways are involved in the regulation of Msr1-mediated lipid induced inflammation. (**a**) Representative confocal microscopy image of lipid uptake, assayed by Oil-red-O-staining. (**b**) Quantification of lipid uptake assayed by absorbance measurement at 518 nm, in BMDMs from WT and *Msr1*$^{-/-}$ aged-matched male mice (**c**) Quantification of lipid uptake in WT BMDMs with 10µg/ml anti-Msr1 monoclonal antibody (2F8) for 1 h. (**d**) Gene ontology pathways enriched based on up-regulated proteins in total cell lysates of WT BMDMs from male aged-matched mice stimulated with SFA (1 mM palmitic acid) for 12 hrs compared to *Msr1*$^{-/-}$ BMDMs from male aged-matched male mice analysed by MS/MS-based proteomics. Data are presented as mean ± SEM. *p< 0.05, **p < 0.01, ***p < 0.001, ****p < 0.0001, *ns:* non-significant; unpaired Student's t-test. Scale bars 50 µm.

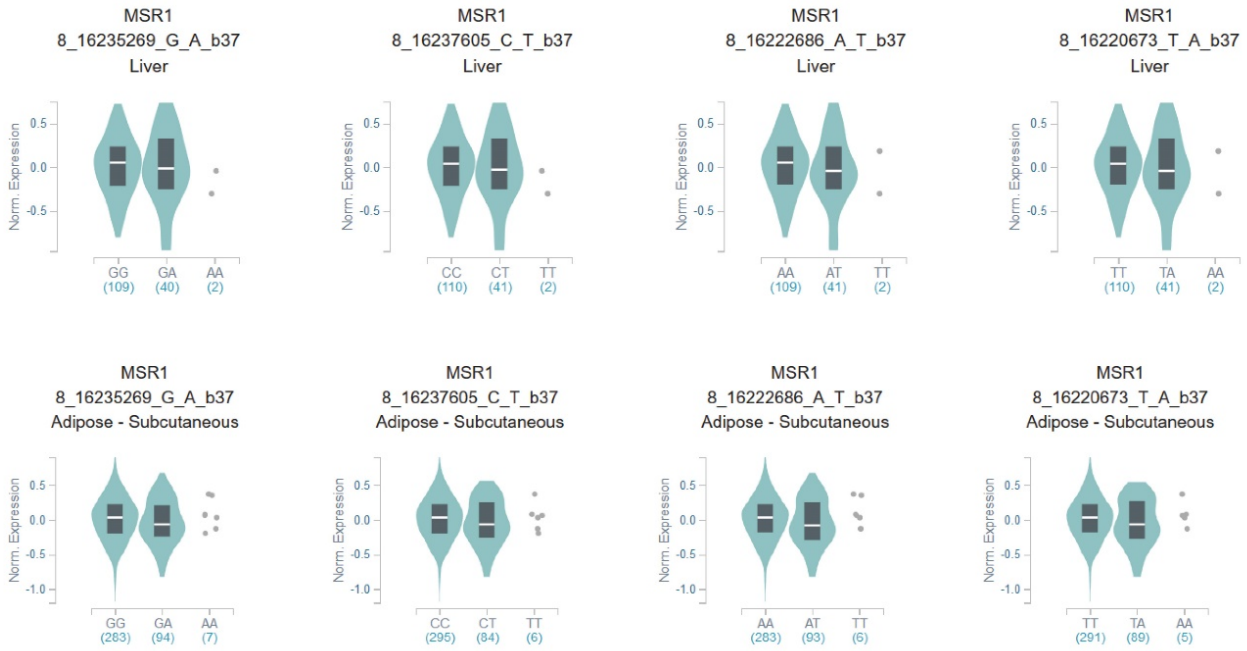

Fig. S6. Expression quantitative trait loci analysis for selected SNPs located in or around the MSR1 locus. No significant effect for rs41505344 (8_16235269_G_A_b37), rs59864667 (8_16237605_C_T_b37), rs55951887 (8_16222686_A_T_b37) and (rs12541232 8_16220673_T_A_b37) on the expression of mRNA *MSR1* was observed in human non-diseased liver (n=151) or subcutaneous adipose tissue (n=384) using the GTex database.